Experimental investigation of self-sustained thermoacoustic instabilities in pure hydrogen swirling flames

Nicolas Vaysse, D. Durox, Ronan Vicquelin, Sébastien Candel, Antoine Renaud

▶ **To cite this version:**

Nicolas Vaysse, D. Durox, Ronan Vicquelin, Sébastien Candel, Antoine Renaud. Experimental investigation of self-sustained thermoacoustic instabilities in pure hydrogen swirling flames. Symposium on Thermoacoustics in Combustion: Industry meets Academia (SoTiC 2023), CAPS, ETH Zürich, ZHAV, Sep 2023, Zürich, Switzerland. hal-04564503

HAL Id: hal-04564503
https://hal.science/hal-04564503v1

Submitted on 30 Apr 2024

HAL is a multi-disciplinary open access archive for the deposit and dissemination of scientific research documents, whether they are published or not. The documents may come from teaching and research institutions in France or abroad, or from public or private research centers.

L'archive ouverte pluridisciplinaire **HAL**, est destinée au dépôt et à la diffusion de documents scientifiques de niveau recherche, publiés ou non, émanant des établissements d'enseignement et de recherche français ou étrangers, des laboratoires publics ou privés.

Distributed under a Creative Commons Attribution 4.0 International License

Symposium on Thermoacoustics in Combustion: Industry meets Academia (SoTiC 2023)
Sept. 11 - Sept. 14, 2023
Zürich, Switzerland
©The Author(s) 2023

Experimental investigation of self-sustained thermoacoustic instabilities in pure hydrogen swirling flames

Nicolas Vaysse[1], Daniel Durox[1], Ronan Vicquelin[1], Sébastien Candel[1], Antoine Renaud[1]

Abstract

The replacement of hydrocarbon fuels in energy production and aeronautical applications by hydrogen raises issues linked to its enhanced reactivity, broad flammability limits and augmented burning velocity. Hydrogen flames may also feature specific sensitivity to acoustic disturbances that may lead to combustion instabilities. This problem is examined in the present work in the case of a single flame formed by a swirling injection unit where hydrogen is injected in cross-flow to enhance mixing to reduce hotspots. Self-sustained oscillations (SSOs) are observed using optical diagnostics and acoustic pressure measurements. It is shown that changes in flame shape during one oscillation cycle feature a periodic attachment and detachment of the flame from the injector, and aerodynamic disturbances enhancing flame wrinkling. The influence of thermal power and global equivalence ratio is investigated and it is shown that unstable oscillations arise when the system is operated in an intermediate thermal power regime where the flame alternates between lifted and attached configurations. Investigations of the effect of swirl number and recess of hydrogen injection with respect to the chamber backplane show that the unstable range is diminished when the recess takes large values and also when the swirl number is increased.

Keywords

Hydrogen flames, Swirling Flows, Self-sustained oscillations, Cross-flow injection

Introduction

Current industrial objectives of replacing traditional hydrocarbon fuels by hydrogen-enriched blends or pure hydrogen require new injection schemes and combustor architectures, that will enable a stable combustion and ensure low NOx emissions. The present work is aimed at examining combustion dynamics issues leading to instabilities of an injection unit that relies on cross-flow injection of hydrogen in a swirled airflow. This configuration is investigated for its capacity to induce a sufficient level of premixing and to establish stable flames anchored at a distance from the injection unit. It was also found that this system features unstable ranges of operation depending on the global equivalence ratio and thermal power values. A first objective of the present study is to characterize these unstable ranges in terms of flame shape, pressure and heat release rate fluctuations. The second objective is to examine effects of geometrical parameters and in particular those defining the swirler (and its swirl number) and the hydrogen injection location with respect to the chamber backplane.

At this stage it is natural to review the literature dealing with the combustion dynamics of flames formed by hydrogen enriched fuel streams and that considering pure hydrogen injection cases. Most of these studies indicate that the addition of hydrogen to gaseous methane that is considered for gas turbines and the use of hydrogen as a fuel in aeroengines raises dynamical issues. The increase of burning velocity and the broader flammability limits corresponding to hydrogen enriched natural gas tend to promote flashback which may occur for example at ignition as a result of the overpressure induced by the rapid reaction of fresh mixture in the chamber[1–3]. This phenomenon is also known for annular configurations[4,5]. Flashback may also be induced during steady operation by the overheating of combustor walls. The change in fuel composition with the addition of hydrogen with higher exothermic power may also enhance the flame sensitivity to incoming disturbances and modify the thermoacoustic coupling between the flame and the chamber. A first mechanism is the reduction of flame size due to the higher burning velocity, and greater resistance to strain rate[6]. Hydrogen enrichment may also induce transitions from "V" to "M" flame shapes observed at lower equivalence ratios[7], with more compact flames[8,9]. The flames become even shorter at high ambient pressures as observed by[8,10]. Flames enriched with hydrogen are characterized by a reduced time delay between upstream flow perturbations and the burning region, a feature that is reflected in the Flame Transfer Functions (FTF) which exhibit a reduction in the phase slope[10–12] with a shift in the characteristic frequencies of methane-air flames enriched with hydrogen[13]. The change in frequency is also a consequence of flame properties

[1]Laboratoire EM2C, CNRS, CentraleSupélec, Université Paris-Saclay, 3, rue Joliot Curie, 91192 Gif-sur-Yvette cedex, France

Corresponding author:
Nicolas Vaysse, Laboratoire EM2C CentraleSupélec, 8-10 rue Joliot-Curie, 91190 Gif-sur-Yvette, France
Email: nicolas.vaysse@centralesupelec.fr

such as burning velocity and adiabatic temperature[14,15]. Gain reductions in the FTF have been reported in both experimental and numerical swirled configurations when the hydrogen content is augmented[10,12,16–18]. This might eventually reduce the sensitivity of such flames to disturbances. The possibility of using hydrogen pilot injection in active control of instabilities was investigated on this basis[17–20]. A constructive coupling of hydrogen combustion with vortex shedding was observed both experimentally and numerically[10,12,21,22]. Experiments have further underlined the complex dependency of hydrogen content on the control itself, since an increase in hydrogen concentration could lead to an increase in heat release rate fluctuations or to enhanced acoustic damping[23,24].

The previous studies were mainly carried out in single injector configurations. Multiple injection systems have also revealed a strong dependency of the triggering of thermoacoustic instabilities with respect to the hydrogen content. Azimuthal mode shifting is observed in the NTNU annular chamber[23], where the inhibitor effect of high hydrogen enrichment is explained to be a result of the cancellation taking place between distinct out-of-phase regions in the flame[25]. Both experiments on can-annular configurations[26] and micromix simulations[27] have shown an enhancement of the thermoacoustic coupling at high frequencies. A low-order model was used to predict growth rate in the low-frequency range implying that combustors using hydrogen micromix injection units were less unstable than lean premixed prevaporized kerosene configurations[27].

The combustion dynamics of systems using pure hydrogen injection is less well documented. There are however indications that multi-slit configurations designed to avoid flashback may also give rise to high-frequency transverse modes[28,29] and to low frequency axial modes.

It is also worth noting that some recent investigations underline the influence of the injection unit characteristics and geometrical parameters but that these studies were only carried out with hydrocarbon fuels. It is found for example that the amplitude and frequency of oscillation change with the atomizer recess[30] and that the combustion dynamics are influenced to a large extent by the injector swirl number[31,32]. Measurements with a variable swirler[33] indicated that it was possible to change the combustion dyamics as a function of the swirl number S. In this study, a higher value of S tended to trigger instabilities at high frequency whereas at moderate swirl levels the flame was stable or exhibited weak instabilities in the low frequency range. Experimental work carried out with different swirlers in the case of spray flames[34] confirmed that combustion instabilities generally corresponded to injectors with higher values of the swirl number.

This brief review of the literature indicates that it is worth examining pure hydrogen injection, specifically consider combustion instabilities as a function of injection unit parameters and study the nature of the coupling observed between such flames and acoustic modes of the system. The present article reports experiments that focus on the special case of cross-flow injection of hydrogen in a swirling stream of air. The experimental setup is briefly described (see[35,36] for more details). Self-sustained oscillations are then characterized through optical diagnostics and acoustic pressure measurements. The domain of instability is then explored with respect to the global equivalence ratio and to the thermal power. Effects of the recess of the hydrogen injection ports and of swirl number are investigated in the last section of this article.

Experimental setup

The experimental facility is derived from the SICCA burner at EM2C Lab, previously used for premixed and spray hydrocarbon combustion. The schematic drawing of this system is shown in Fig. 1. Gaseous hydrogen is injected in cross-flow in a swirled air flow. This kind of injection is commonly used in supersonic combustion engines where the flow is essentially oriented in the axial direction. The penetration of hydrogen is however limited by its low density. In the present arrangement, mixing is enhanced by the swirling air stream[36]. A similar scheme was used for an injection of a blend of CH_4 with H_2[37]. The injector, denoted as CFI-X2, comprises an 11 mm slender cone that is slightly longer than the one used in[35,36]. Six radial channels of diameter 1.5 mm are drilled in its base and convey gaseous hydrogen. The tangential swirler can be easily taken out and replaced to vary the swirl number, while the injector recess, defining the distance h_r between the hydrogen injection orifices with respect to the outlet, can be modified with a screw system. The combustion chamber is composed of a 150 mm long quartz tube with a 68.5 mm diameter. A 15 mm high metal piece is placed beneath this tube to allow pressure measurements in the vicinity of the chamber backplane.

Flame images are captured using a Princeton Instruments PI-MAX4 intensified camera, equipped with an Asahi Spectra 310 mm filter for OH* chemiluminescence or a glass plate to cut UV light from OH* and only keep the spectral range corresponding to visible light emission from hot burnt products, either hot water vapor or excited hydrogen peroxide[38,39].

Investigation of self-sustained oscillations

The injection unit is first set up with a recess $h_r = 11.1$ mm and a 707 swirler, characterized by a conventional swirl number $S = 0.60$ and a pressure loss coefficient $\sigma = \Delta p/[(1/2)\rho U_b^2] = 3.25$, with U_b the axial bulk velocity at the injector outlet (this swirler belongs to a family of such units characterized by their head loss coefficient and swirl number, see[40]). An example of flame dynamics for an unstable case is analyzed in this section. The thermal power is $\mathcal{P}_{th} = 2.7$ kW and the global equivalence ratio is $\phi = 0.5$. Self-sustained oscillations occurring at a frequency of 899 ± 4 Hz, correspond to a quarter-wave longitudinal mode of the combustion chamber. Phase-averaged OH* emission images of this instability are presented in Fig. 2. The phase $\theta = 0°$ corresponds to a crossing at 0 of the pressure oscillation inside the plenum (MP in Fig. 1a) with a rising slope. These phase-averaged images reveal a longitudinal motion of the flame characterized by a cyclic detachment and reattachment on the injector conical piece. A toroidal vortex formation is identified at the top of the flame front. The vortex in which

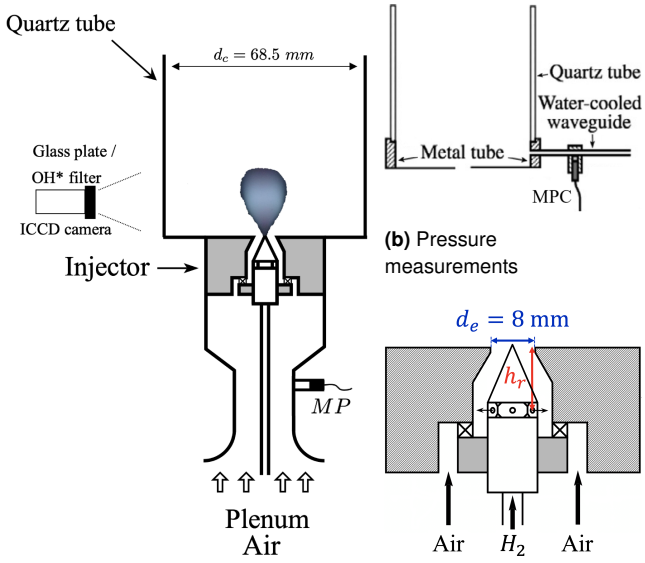

(a) Full burner **(b)** Pressure measurements **(c)** CFI-X2

Figure 1. Experimental setup: full burner for (a) flame visualization, (b) pressure measurements, and (c) CFI-X2. The height h_r is the recess between the injection holes and the chamber backplane.

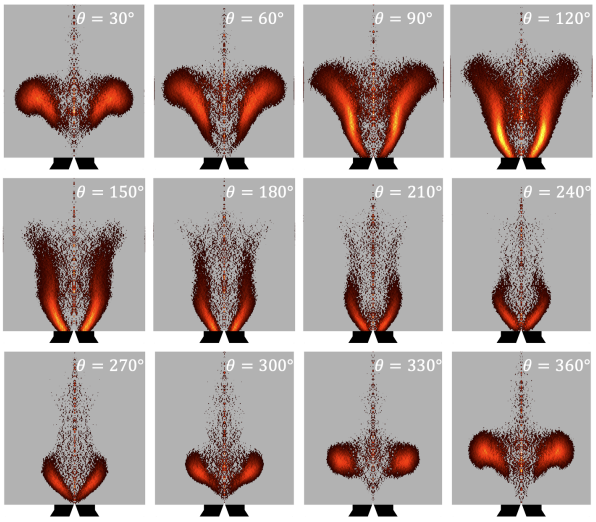

Figure 2. Phase averaged OH* chemiluminescence images of the unstable flame at $\mathcal{P}_{th} = 2.7$ kW and $\phi = 0.50$, obtained with the baseline geometry: $S = 0.60$ and $h_r = 11.1$ mm. The phase angle is denoted by θ. Injector parts are represented in white, and the invisible region in black. The images are obtained after an Abel deconvolution.

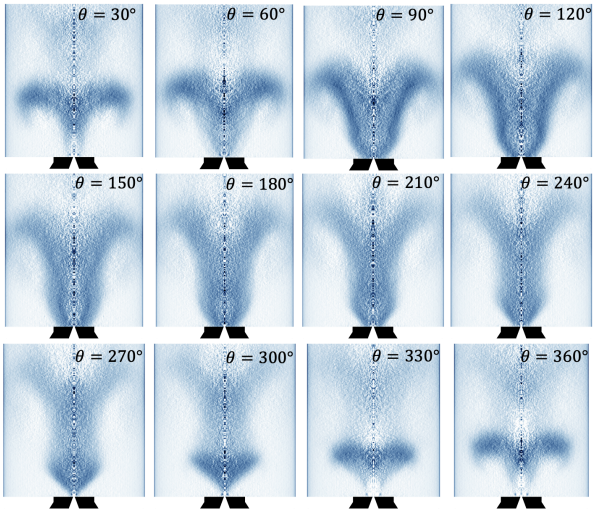

Figure 3. Phase averaged visible emission images of the unstable flame at $\mathcal{P}_{th} = 2.7$ kW and $\phi = 0.50$, obtained with the baseline geometry: $S = 0.60$ and $h_r = 11.1$ mm. The phase angle is denoted by θ. Injector parts are represented in white, and the invisible region in black. The images are obtained after an Abel deconvolution.

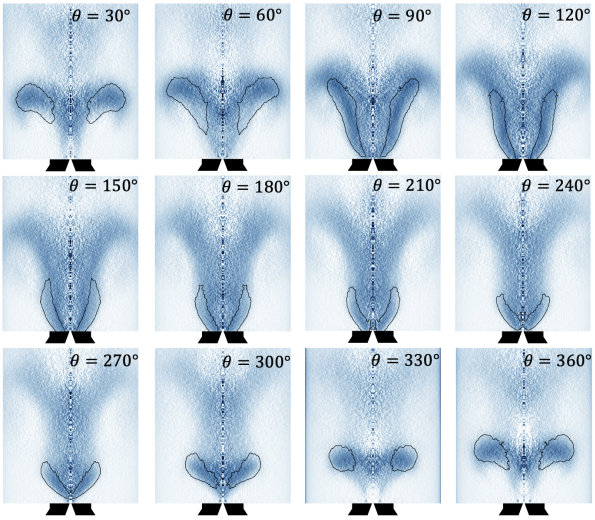

Figure 4. Contours of the OH* emission superimposed to the phase averaged visible emission images of the unstable flame at $\mathcal{P}_{th} = 2.7$ kW and $\phi = 0.50$, obtained with the baseline geometry: $S = 0.60$ and $h_r = 11.1$ mm. The phase angle is denoted by θ. Injector parts are represented in white, and the invisible region in black. The images are obtained after an Abel deconvolution.

the flame is rolled up is convected upwards together with the stream of fresh reactants.

Another view of this thermoacoustic instability can be obtained by replacing the OH* filter with an UV-cut filter (glass plate). Since water vapor radiates in near infrared and infrared regions and the blue emission is suspected to be produced by visible burnt gases[39], this filter enables to localize the burnt gases region. The corresponding phase-averaged images are presented in Fig. 3.

At first, burnt gases radiating in the visible range are located inside the reactive front materialized by OH* emission and are always in contact with the injector. Burnt gases might also have been present in the outer recirculation zone but the signal level recorded in Fig. 3 in that zone remains low probably because of the low ambient temperature in that region. Although the flame front, visualized by OH*, detaches from the injector between $\theta = 270°$ and $\theta = 60°$ (Fig. 2), the burnt gas region radiating visible light remains attached during the whole period.

Second, the intensity of the visible emission is fairly homogeneous over the flame length, except for regions that are in the flame front vicinity where the signal is slightly stronger. This can be seen in Fig. 4 where the contour of OH* images obtained with Otsu thresholding method has been superimposed to the visible blue emission. This

could be explained either by the presence of visible burnt gases directly next to the flame front, or by molecular OH radicals involved in the suspected reactions for the blue continuum, as proposed by Fiala and Sattelmayer[39]. Indeed, in conclusion of this work, the authors show that the OH* and blue emissions are located in the same zones, and that the role of OH radicals in both mechanisms (de-excitation of OH* and hydrogen peroxide formation) can explain this co-location. They are also suggesting that both radiations can be used to describe the dynamic behavior. In the present study, the advection of hot burnt gases downstream the flame front leads to a wider blue emission zone than the OH* zone.

The visible emission clearly shows the trace of the toroidal vortex shedding due to the instability. Indeed, it is possible to see in Fig. 4 that the vortex periodically produced in the flame front vicinity keeps propagating downstream, and the phase-averaged images allow to compute the phase velocity of these vorticity waves : at $\theta = 300°$, one can clearly see both vortices, separated by 18.7 mm, which corresponds to a phase velocity $V_\varphi = 16.7\,\mathrm{m\,s^{-1}} = 0.53U_b$, i.e. half the bulk velocity.

Space-time analysis of the Rayleigh source term

It is next interesting to use the phase average images in a space-time analysis of the Rayleigh source term. This term appears in the acoustic energy balance equation. If its sign is positive acoustic energy is being added to the oscillation by the unsteady combustion process. If its sign is negative, energy is being subtracted and the oscillation is damped.

Under some fairly general assumptions, the acoustic energy balance takes the form

$$\frac{\partial \mathcal{E}}{\partial t} + \boldsymbol{\nabla} \cdot \mathcal{F}_a = \mathcal{S} - \mathcal{D} \tag{1}$$

where $\mathcal{E}$, $\mathcal{F}_a$, $\mathcal{S}$ and $\mathcal{D}$ are repectively, the acoustic energy density, acoustic energy flux, Rayleigh source term and volumetric damping term representing dissipation processes:

$$\mathcal{E} = \frac{1}{2}\frac{p'^2}{\rho_0 c^2} + \frac{1}{2}\rho_0 v'^2 \tag{2}$$

$$\mathcal{F}_a = p'\boldsymbol{v}' \tag{3}$$

$$\mathcal{S} = \frac{\gamma - 1}{\rho_0 c^2} p' \dot{q}' \tag{4}$$

The previous expressions correspond to instantaneous quantities. The following developement is focused on the source term $\mathcal{S}$.

It can be assumed that the OH* emission is a rough tracer of the heat release rate, at least that the two quantities evolve in phase. One may then deduce the spatial distribution of this last quantity at different phases during the cycle of oscillation. This implies that combustion essentially takes place in the premixed mode which is admittedly an approximation because the flow is not perfectly premixed and the equivalence ratio is not constant. There is however a relation between the light emitted by OH* radicals and the heat release rate as implied by the fact that the phase average OH* emission images follow the flame dynamics and reveal the motion of the reactive layer. In what follows we tentatively assume that the phase average relative fluctuation in volumetric heat release rate is proportional to the phase average relative fluctuation in OH* light intensity. This will have to be validated by further experiments. In the problem at hand the period averages and time average of light intensity are axisymmetric because the mean flow and its modulation by the longitudinal pressure mode have a rotationally symmetry. We now consider a cycle of oscillation with a period T and N instants during this cycle, $t_n = T/N$, where the light emission distribution is determined by taking period averages. Let $I(r, z, t_n)$ designate the period average light distribution at t_n. The mean light intensity distribution may be obtained by summing the period average images over all instants during the cycle

$$\overline{I}(r, z) = \frac{1}{N}\sum_{n=0}^{N-1} I(r, z, t_n) \tag{5}$$

The period average fluctuation distribution may then be obtained by subtraction the mean distribution from the period average distributions corresponding to the various instants t_n :

$$\widetilde{I}(r, z, t_n) = I(r, z, t_n) - \overline{I}(r, z) \tag{6}$$

It is also useful to define the total light intensity level

$$I_0 = \int \overline{I}(r, z) 2\pi r dr dz \tag{7}$$

Using the assumption concerning the relation between volumetric heat release rate fluctuations and light intensity fluctuations, one may write:

$$\frac{\widetilde{\dot{q}}(r, z, t_n)}{\dot{Q}_0} \simeq \frac{\widetilde{I}(r, z, t_n)}{I_0} \tag{8}$$

For the space-time analysis the key idea is to keep the axial coordinate and the time instants t_n. This is achieved by integrating the period average distributions with respect to the radial coordinate. It is also convenient to sum the light intensity in thin axial slices δz. One obtains in this way:

$$\frac{\langle I(z, t_n)\rangle}{I_0} = \int_z^{z+\delta z}\int_0^R \frac{\widetilde{I}(r, z, t_n)}{I_0} 2\pi r dr dz \tag{9}$$

Since the pressure fluctuation only depends on z and t and remembering that $\rho_0 c^2 = \gamma p_0$ where p_0 is the ambient pressure, one may express the Rayleigh source term integrated in the radial direction and in a slice δz as

$$\frac{\gamma - 1}{\rho_0 c^2}\int_0^R p'\dot{q}' 2\pi r dr = \dot{Q}_0 \frac{\gamma - 1}{\gamma}\frac{\widetilde{p}(z, t_n)}{p_0}\frac{\langle I(z, t_n)\delta z\rangle}{I_0} \tag{10}$$

One can then plot a Rayleigh index based on the OH* light emission and on the pressure recorded at the chamber backplane using the previous expression (Fig. 5). This index defines the source term integrated over a cylindrical volume of radius R and thickness δz. Constructive coupling between heat relase rate and pressure occurs in the vortex region and in the vicinity of the flame anchor during the reattachment step that follows. During the short duration where detachment of the flame takes place, the Rayleigh index becomes negative and tends to damp the instability. The map shows that the point of maximum correlation between pressure and OH* intensity fluctuations is located at

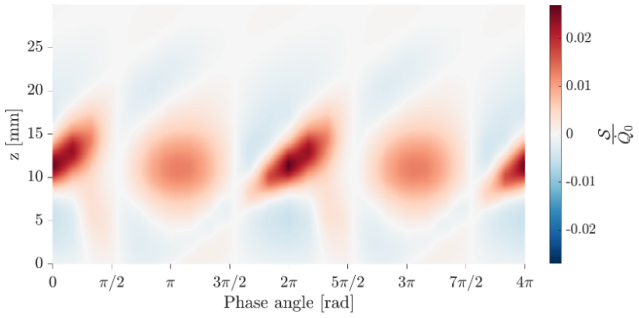

Figure 5. Temporal height-averaged maps of estimated Rayleigh index, computed as the product of OH*intensity fluctuations and pressure fluctuations. The results have been interpolated in time from the phase-averaged images. Axial variations of the fluctuations in OH* intensity are based on radius-weighted average of the Abel-inverted OH*signal at each height.

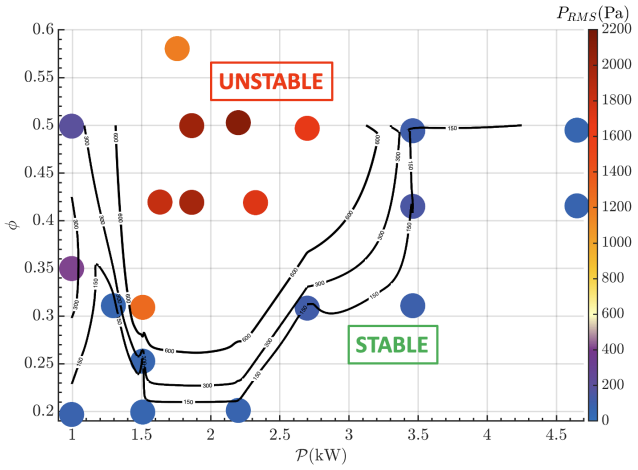

(a) Pressure P_{RMS}

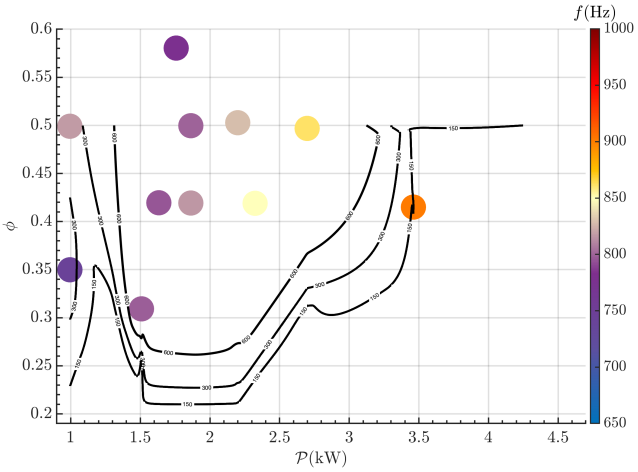

(b) Frequency f

Figure 6. Stability maps for the baseline geometry: $h_r = 11.1$ mm and swirler 707. (a) Pressure oscillation amplitude and (b) Frequency

the flame top and corresponds to the toroidal vortex pattern described previously. The zone of positive Rayleigh index is then rapidly shifted downwards, and the flame lift-off sequence is characterized at the flame foot by rising OH* fluctuations coupled with negative pressure values. However, the level of negative Rayleigh index is much smaller than the level of positive Rayleigh index values. Furthermore, this negative zone sequence occurs at a time where a strong amplification is taking place further downstream at a distance of about 7 mm, corresponding to the flame tip extinguishing (from $\theta = 150°$ and $\theta = 270°$ in Fig. 2). This movement, that appears in red in Fig. 5 between $3\pi/4$ and $3\pi/2$, is slower than the flame foot attachment (between $\pi/4$ and $\pi/2$) and is delayed in time with respect to it. This zone corresponds to lower OH* intensity than the mean intensity and negative pressure, which leads to a positive value of the Rayleigh index. When the Rayleigh index is integrated over the whole flame, it is found to be positive. This corresponds to a source of acoustic energy to the resonant mode. If this addition is sufficiently large and exceeds the damping level, oscillations are sustained.

Effect of operating conditions on flame stability

The instability that has been previously examined occurs in an intermediate domain of operation where the thermal power is moderate and the bulk velocity is relatively low. This domain is between the zone where the flames are attached (at low thermal power and low equivalence ratio), and the zone where the flames are lifted (high thermal power values)[36]. Systematic recordings of pressure and OH* measurements for various thermal powers and equivalence ratio can be used to draw a stability map of the system equipped with the CFI-X2 injector and operating under pure hydrogen injection. Figure 6 includes two maps, the first one showing the root mean square (RMS) of the pressure oscillations, and the second one presenting the frequency of the thermoacoustic oscillations. The pressure RMS value at the backplane of the chamber reaches 2000 Pa in the strongest instability conditions.

The isolines plotted in black on these maps corresponds to levels of 150, 300 and 600 Pa, that are respectively 8, 14 and 20 dB above the baseline given by fully stable flames in terms of sound pressure level. The flames are considered as stable if the pressure RMS value is below 150 Pa and if the pressure signal shows no harmonic oscillations. The unstable range is located at high equivalence ratio and intermediate power, and delimited by $\phi > 0.3$ and $1.5 < \mathcal{P}_{th} < 3$ kW. Inside the unstable range, the frequency is deduced from the power spectral density of the pressure signal, using Welch's method. Figure 6b shows that the frequency of these self-sustained oscillations lies between 750 Hz and 880 Hz. This is consistent with a coupling by the first longitudinal mode of the combustion chamber :

$$f = \frac{c}{4(l_c + 0.4d_c)} \tag{11}$$

where $0.4d_c$ represents the open-end correction of a cylindrical tube outlet, l_c being the chamber length and c the mean speed of sound in the chamber. The frequency of the instability obtained for $\phi = 0.5$ and $\mathcal{P}_{th} = 2.7$ kW is slightly lower here than the frequency detected during phase-averaged imaging in Fig. 2 because of the additional 15 mm length brought by the chamber microphone port.

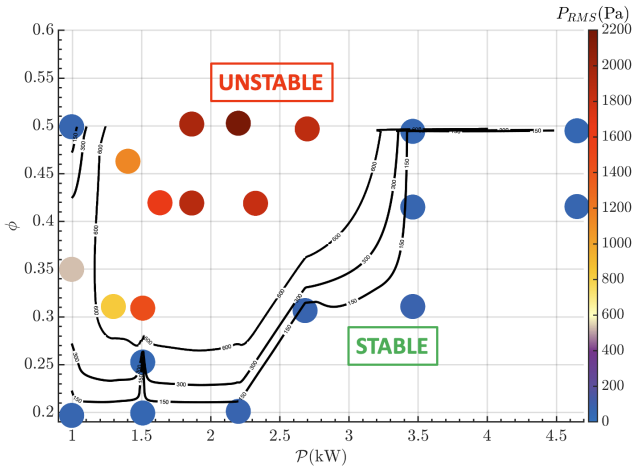

(a) $h_r = 10.1$ mm.

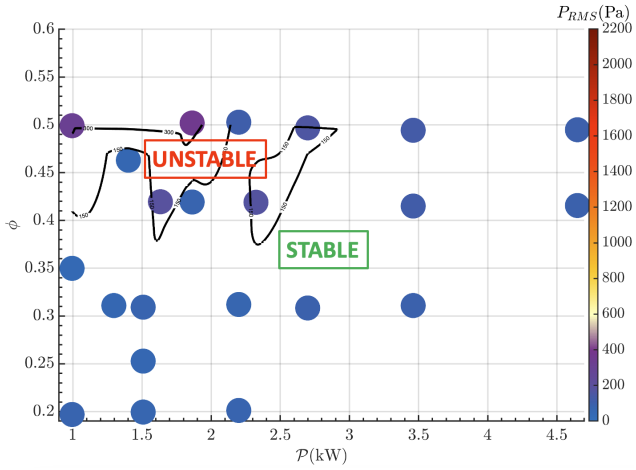

(b) $h_r = 14.1$ mm.

Figure 7. Stability maps plotted in pressure oscillation amplitude for swirler 707. (a) $h_r = 10.1$ mm and (b) $h_r = 14.1$ mm.

Effect of the injector recess on the triggering of SSOs

It is now interesting to consider the effect of recess and, for that, place the hydrogen injection ports at two other locations: a higher position at $h_r = 10.1$ mm and a lower position at $h_r = 14.1$ mm. Resulting stability maps are shown in Fig. 7.

The levels obtained with the recess length $h_r = 10.1$ mm are almost exactly those obtained with the baseline geometry (Fig. 7a). The unstable zone, bounded by the 150 Pa isoline, is slightly broader in the low power region. The pressure RMS values are similar to those obtained at $h_r = 11.1$ mm, indicating that the recess length has a low impact when the injector is close to the outlet. However, the pressure fluctuation levels measured for the highest recess length $h_r = 14.1$ mm are much lower. As visible in Fig. 7b, the pressure fluctuations remain below 500 Pa for all operating points. This emphasizes the nonlinearity of the dependency of SSOs amplitudes with respect to the injector recess and indicates that the thermoacoustic instabilities are strongly reduced when the injector is moved upstream.

One can measure the phase difference between the pressure and OH* intensity fluctuations at the flame level. A cross power spectral density (CPSD) is computed between the signals of pressure and OH* intensity. Gain, phase and coherence values are determined at the frequency peak given by this CPSD. This being done for all the operating points, results for the phase shift are presented for $h_r = 11.1$ mm and $h_r = 14.1$ mm in Fig. 8. They show that in the unstable region bounded by the 150 Pa isoline, the phase shift values remain close to $-\pi/4$ in the low recess case, while the high recess case is characterized by lower phase delays, spread between $-3\pi/4$ and $-\pi$ in the same operating zone. This indicates that in that zone, the highest recess length leads to out-of-phase fluctuations between OH* intensity and pressure. Considering operating point A in Fig. 8, which corresponds to $\phi = 0.50$ and $\mathcal{P}_{th} = 1.86$ kW, the flame is unstable for a recess length $h_r = 11.1$ mm. It is one of the most unstable points using this baseline configuration with a RMS pressure equal to 2000 Pa. For this flame, Fig. 8a gives a phase shift $\varphi^1_{P'-I'_{OH^*}} = -0.72$ rad. When the recess length is increased up to 14.1 mm, this point becomes less unstable (around 400 Pa) as shown in Fig. 7b. A similar evolution can be observed for point B where the fluctuations drop from 1600 Pa to 200 Pa. An odd observation for these two points is that the phase shift falls to $\varphi^2_{P'-I'_{OH^*}} = -2.42$ rad for point A and $\varphi^2_{P'-I'_{OH^*}} = -2.73$ rad for point B, meaning that the pressure fluctuations and the OH* signals are out of phase while some pressure fluctuations, albeit limited, can be witnessed. At first sight, this seems to contradict the Rayleigh criterion but this can be explained when one looks at the shape and behavior of the flame for operating point A shown in Fig. 9. Indeed, during an important part of this cycle, the flame is hidden inside the injector and is thus not visible by the photomultiplier. Therefore, the OH*signal from the photomultiplier is clearly not linked to the global heat release rate of the flame in this case.

Impact of the swirl number

The swirler effects are now investigated by replacing swirler 707 by a swirler inducing a stronger swirling flow (called 726) keeping the recess length $h_r = 11.1$ mm. The swirl number of this new swirler is $S = 0.74$ and the pressure loss coefficient is also increased $\sigma = 5.47$[40]. Both properties exceed those of swirler 707 ($S = 0.60$ and $\sigma = 3.25$). The map shown in Fig. 10 features an unstable zone, still located at high equivalence ratio and intermediate thermal power. The frequencies visible in Fig. 10b have the same order of magnitude as previously, which is consistent with the chamber length being kept constant. However, the level of pressure fluctuations is far below that reached using swirler 707: the maximum is at 1200 Pa instead of 2200 Pa in the low swirl number case, and the 150 Pa isoline encloses a smaller unstable domain than with swirler 707. This seems to be at variance with observations made on this burner for spray flames and at lower frequencies of oscillation[34], but the mixing and the flame shape are very different from the spray flames of the cited article. The hydrogen flames of this study have very different dynamics and characteristic transport times of flow disturbances on the flame, which leads to this situation: an increase in the swirl number corresponds

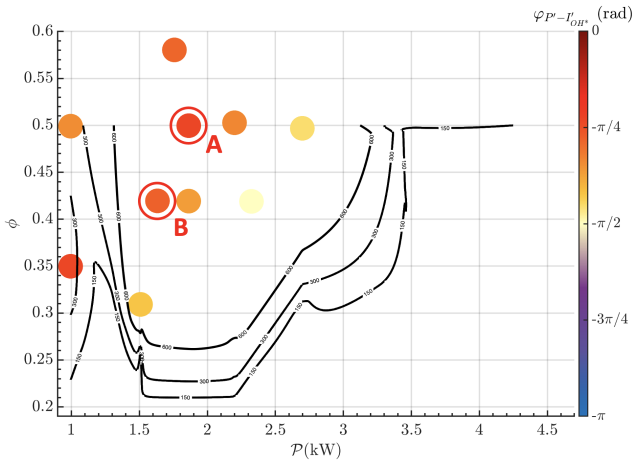

(a) $h_r = 11.1$ mm

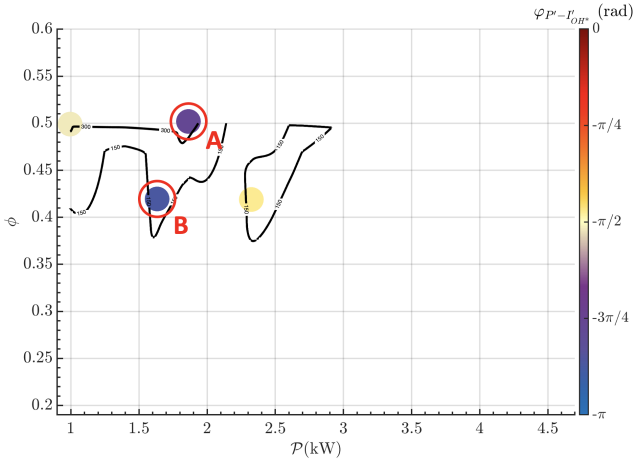

(b) $h_r = 14.1$ mm

Figure 8. Mapping of the phase shift between pressure fluctuations p' and OH* intensity fluctuations I'_{OH^*} for swirler 707. (a) Recess length $h_r = 11.1$ mm and (b) $h_r = 14.1$ mm. The phase value is only plotted when the coherence level between the two signals is high ($\gamma^2 > 0.9$) and when the pressure RMS value is greater than 150 Pa.

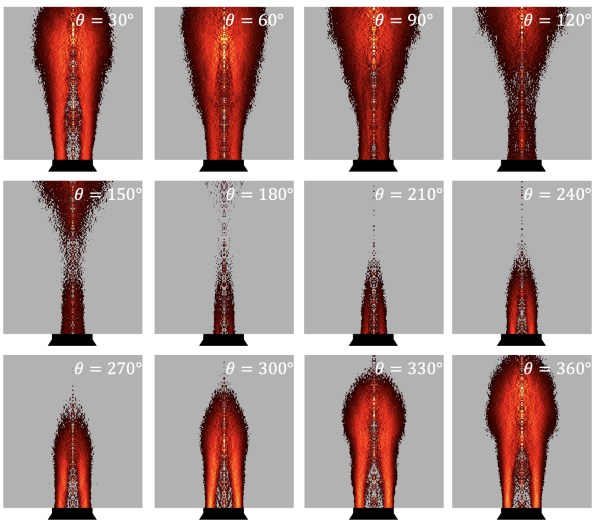

Figure 9. Phase averaged OH* chemiluminescence images of the unstable flame A at $\mathcal{P}_{th} = 1.83$ kW and $\phi = 0.50$, obtained with the geometry $S = 0.60$ and $h_r = 14.1$ mm. The phase angle is denoted by θ. Injector parts are represented in white, and the invisible region in black. The images are obtained after an Abel deconvolution.

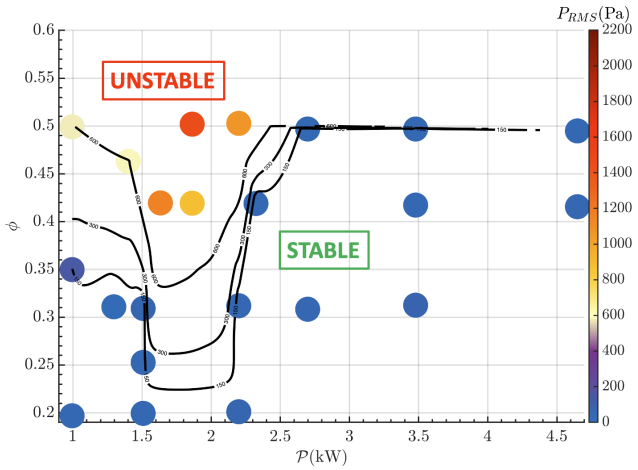

(a) Pressure P_{RMS}

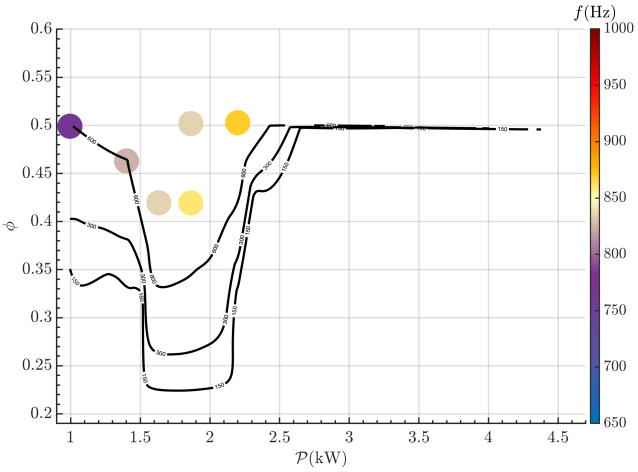

(b) Frequency f

Figure 10. Stability maps corresponding to swirler 726. (a) Pressure oscillation amplitude and (b) Frequency. $h_r = 11.1$ mm.

in the present experiment to a reduction in thermoacoustic instability.

The flames obtained using swirler 707 and 726 have different shapes. In stable operation (above $\mathcal{P}_{th} = 3$ kW) , while the first one is lifted above the injector cone, the second one is attached to the cone and wide open. This may induce different responses of the flame to acoustic disturbances. The phase difference between pressure and OH* intensity fluctuations is computed for both swirlers and results are displayed in Fig. 11. A first observation is that on the high-pressure border of the unstable zone, the phase difference decreases between swirler 707 and swirler 726. This is consistent with the reduction of the unstable zone: indeed, considering point B in Fig. 11, the phase shift decreases from $\varphi^1 = -0.87$ rad to $\varphi^2 = -1.19$ rad and the level of pressure fluctuations is reduced from 1900 Pa to 1100 Pa RMS (Fig. 6a and 10a). For operating point C, which corresponds to $\phi = 0.42$ and $\mathcal{P}_{th} = 1.86$ kW, the phase also slightly decreases when using swirler 726, from -1.16 rad to -1.49 rad.

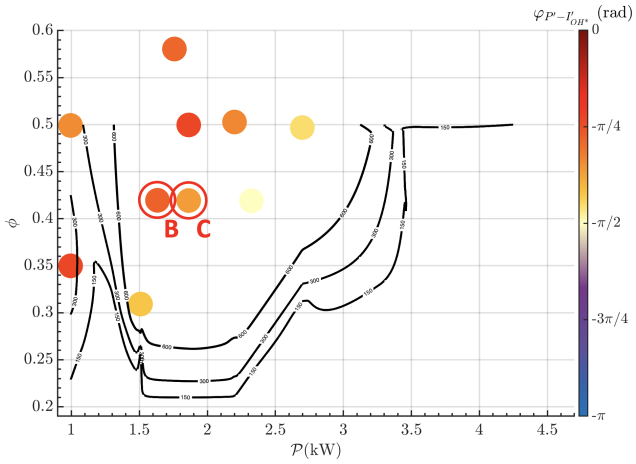

(a) Swirler 707

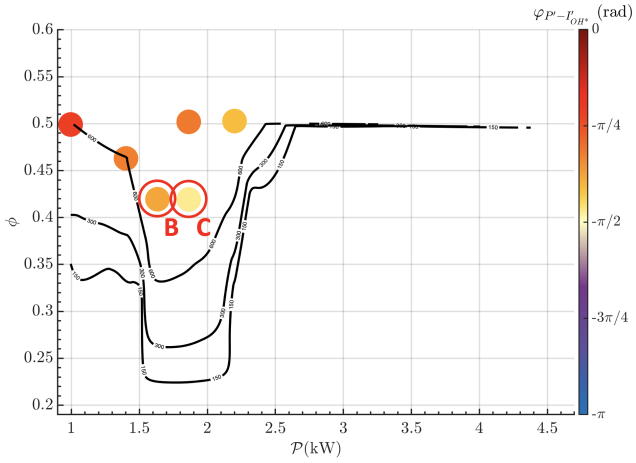

(b) Swirler 726

Figure 11. Mapping of the phase shift between pressure fluctuations p' and OH* intensity fluctuations I'_{OH^*} at a recess length $h_r = 11.1$ mm using (a) Swirler 707 and (b) Swirler 726. Only the operating points leading to pressure fluctuations greater than 150 Pa and coherence function $\gamma^2 > 0.9$ between the two signals are kept.

Conclusion

Combustion instability of pure hydrogen flames is examined in the case of a cross-flow injection in a swirling stream of air. Systematic experiments indicate that self-sustained oscillations arise in an intermediate range of thermal powers when the flame combines attached-"V" and detached patterns. Light emission imaging in the UV and visible ranges indicates that the burnt gas region is continuously attached to the injector outlet while the flame front is lifted off cyclically. A space-time analysis of the acoustic energy source term carried out by considering pressure and heat release rate signals integrated in the transverse direction indicates that this axial motion corresponds to a constructive coupling between pressure and heat release rate when the reactive region in the flames is convected away from the injection unit. The periodic lift-off that follows is found to be in phase opposition with the pressure oscillation and thus reduces the acoustic energy of the mode.

Changes in the recess of the hydrogen injection section with respect to the outlet indicate that this parameter notably influences the combustion instability process even for relatively small variations. It is shown that with a higher recess length these two signals become out-of-phase. A somewhat unusual phenomenon for this burner was also observed in these experiments in which an increase in the swirl number induces a reduction in the instability level. The change in flame shape with the swirl number induces a change in phase between the OH* intensity and pressure fluctuations with a lower phase at high swirl.

Acknowledgements

This work was partially supported by the FlyHy project of the Agence Nationale de la Recherche (ANR-21-CE05-0008). For open access purposes, a CC-BY license has been applied by the authors to this document and will be applied to any subsequent version up to the author's manuscript accepted for publication resulting from this submission.

References

1. Yahou T, Dawson JR and Schuller T. Impact of chamber back pressure on the ignition dynamics of hydrogen enriched premixed flames. *Symposium (International) on Combustion* 2022; : 9.
2. Aniello A, Poinsot T, Selle L and Schuller T. Hydrogen substitution of natural-gas in premixed burners and implications for blow-off and flashback limits. *International Journal of Hydrogen Energy* 2022; 47(77): 33067–33081. DOI:10.1016/j.ijhydene.2022.07.066. URL https://www.sciencedirect.com/science/article/pii/S0360319922030804.
3. Pers H, Aniello A, Morisseau F and Schuller T. Autoignition-induced flashback in hydrogen-enriched laminar premixed burners. *International Journal of Hydrogen Energy* 2022; DOI:10.1016/j.ijhydene.2022.12.041. URL https://www.sciencedirect.com/science/article/pii/S036031992205755X.
4. Prieur K, Vignat G, Durox D, Schuller T and Candel S. Flame and Spray Dynamics During the Light-Round Process in an Annular System Equipped With Multiple Swirl Spray Injectors. *Journal of Engineering for Gas Turbines and Power* 2019; 141(061007). DOI:10.1115/1.4042024. URL https://doi.org/10.1115/1.4042024.
5. Töpperwien K, Collin-Bastiani F, Riber E et al. Large-Eddy Simulation of Flame Dynamics During the Ignition of a Swirling Injector Unit and Comparison With Experiments. *Journal of Engineering for Gas Turbines and Power* 2021; 143(021015). DOI:10.1115/1.4049297. URL https://doi.org/10.1115/1.4049297.
6. Schimek S, Göke S, Schrödinger C and Paschereit CO. Flame Transfer Function Measurements With CH4 and H2 Fuel Mixtures at Ultra Wet Conditions in a Swirl Stabilized Premixed Combustor. In *Volume 2: Combustion, Fuels and Emissions, Parts A and B* 2012. Copenhagen, Denmark: American Society of Mechanical Engineers. ISBN 978-0-7918-4468-7, pp. 1335–1344. DOI:10.1115/GT2012-69788. URL https://asmedigitalcollection.asme.org/GT/proceedings/GT2012/44687/1335/250535.
7. Shanbhogue SJ, Sanusi YS, Taamallah S, Habib MA, Mokheimer EMA and Ghoniem AF. Flame macrostructures,

combustion instability and extinction strain scaling in swirl-stabilized premixed CH4/H2 combustion. *Combustion and Flame* 2016; 163: 494–507. DOI:10.1016/j.combustflame.2015.10.026. URL https://www.sciencedirect.com/science/article/pii/S001021801500382X.

8. Chterev I and Boxx I. Effect of hydrogen enrichment on the dynamics of a lean technically premixed elevated pressure flame. *Combustion and Flame* 2021; 225: 149–159. DOI:10.1016/j.combustflame.2020.10.033. URL https://www.sciencedirect.com/science/article/pii/S0010218020304533.
9. Aguilar JG, Æsøy E and Dawson JR. The influence of hydrogen on the stability of a perfectly premixed combustor. *Combustion and Flame* 2022; 245(112323). DOI:10.1016/j.combustflame.2022.112323. URL https://www.sciencedirect.com/science/article/pii/S0010218022003388.
10. Kwak S, Choi J, Ahn M and Yoon Y. Effects of hydrogen addition on the forced response of H2/CH4 flames in a dual-nozzle swirl-stabilized combustor. *International Journal of Hydrogen Energy* 2022; 47(65): 28139–28151. DOI:10.1016/j.ijhydene.2022.06.117. URL https://www.sciencedirect.com/science/article/pii/S0360319922027495.
11. Joo S, Kwak S, Lee J and Yoon Y. Thermoacoustic instability and flame transfer function in a lean direct injection model gas turbine combustor. *Aerospace Science and Technology* 2021; 116: 106872. DOI:10.1016/j.ast.2021.106872. URL https://www.sciencedirect.com/science/article/pii/S1270963821003825.
12. Æsøy E, Aguilar JG, Wiseman S, Bothien MR, Worth NA and Dawson JR. Scaling and prediction of transfer functions in lean premixed H2/CH4-flames. *Combustion and Flame* 2020; 215: 269–282. DOI:10.1016/j.combustflame.2020.01.045. URL https://www.sciencedirect.com/science/article/pii/S0010218020300572.
13. Schuller T, Poinsot T and Candel S. Dynamics and control of premixed combustion systems based on flame transfer and describing functions. *J Fluid Mech* 2020; 894: P1. DOI:10.1017/jfm.2020.239. URL https://www.cambridge.org/core/product/identifier/S0022112020002396/type/journal_article.
14. Park J and Lee MC. Combustion instability characteristics of H2/CO/CH4 syngases and synthetic natural gases in a partially-premixed gas turbine combustor: Part I—Frequency and mode analysis. *International Journal of Hydrogen Energy* 2016; 41(18): 7484–7493. DOI:10.1016/j.ijhydene.2016.02.047. URL https://www.sciencedirect.com/science/article/pii/S0360319915305085.
15. Yoon J, Joo S, Kim J, Lee MC, Lee JG and Yoon Y. Effects of convection time on the high harmonic combustion instability in a partially premixed combustor. *Proceedings of the Combustion Institute* 2017; 36(3): 3753–3761. DOI:10.1016/j.proci.2016.06.105. URL https://www.sciencedirect.com/science/article/pii/S1540748916301638.
16. Lim Z, Li J and Morgans AS. The effect of hydrogen enrichment on the forced response of CH4/H2/Air laminar flames. *International Journal of Hydrogen Energy* 2021; 46(46): 23943–23953. DOI:10.1016/j.ijhydene.2021.04.171. URL https://www.sciencedirect.com/science/article/pii/S0360319921016189.
17. Oztarlik G, Selle L, Poinsot T and Schuller T. Suppression of instabilities of swirled premixed flames with minimal secondary hydrogen injection. *Combustion and Flame* 2020; 214: 266–276. DOI:10.1016/j.combustflame.2019.12.032. URL https://linkinghub.elsevier.com/retrieve/pii/S0010218019305905.
18. Ghani A and Polifke W. Control of intrinsic thermoacoustic instabilities using hydrogen fuel. *Proceedings of the Combustion Institute* 2021; 38(4): 6077–6084. DOI:10.1016/j.proci.2020.06.151. URL https://www.sciencedirect.com/science/article/pii/S1540748920302315.
19. Barbosa S, de La Cruz Garcia M, Ducruix S, Labegorre B and Lacas F. Control of combustion instabilities by local injection of hydrogen. *Proceedings of the Combustion Institute* 2007; 31(2): 3207–3214. DOI:10.1016/j.proci.2006.07.085. URL https://www.sciencedirect.com/science/article/pii/S1540748906001039.
20. Nam J and Yoh JJ. A numerical investigation of the effects of hydrogen addition on combustion instability inside a partially-premixed swirl combustor. *Applied Thermal Engineering* 2020; 176: 115478. DOI:10.1016/j.applthermaleng.2020.115478. URL https://www.sciencedirect.com/science/article/pii/S1359431120329604.
21. Poinsot TJ, Trouve AC, Veynante DP, Candel SM and Esposito EJ. Vortex-driven acoustically coupled combustion instabilities. *Journal of Fluid Mechanics* 1987; 177: 265–292. DOI:10.1017/S0022112087000958. URL https://www.cambridge.org/core/journals/journal-of-fluid-mechanics/article/vortexdriven-acoustically-coupled-combustion-instab92B33FC9998469063494810940E8B8AD. Publisher: Cambridge University Press.
22. Kangkang G, Boqi X, Yongjie R, Yiheng T and Wansheng N. Three-Dimensional Numerical Analysis of Longitudinal Thermoacoustic Instability in a Single-Element Rocket Combustor. *Frontiers in Energy Research* 2022; 10. URL https://www.frontiersin.org/articles/10.3389/fenrg.2022.835977.
23. Indlekofer T, Ahn B, Kwah YH et al. The effect of hydrogen addition on the amplitude and harmonic response of azimuthal instabilities in a pressurized annular combustor. *Combustion and Flame* 2021; 228: 375–387. DOI:10.1016/j.combustflame.2021.02.015. URL https://www.sciencedirect.com/science/article/pii/S001021802100078X.
24. Zhang J and Ratner A. Experimental study of the effects of hydrogen addition on the thermoacoustic instability in a variable-length combustor. *International Journal of Hydrogen Energy* 2021; 46(29): 16086–16100. DOI:10.1016/j.ijhydene.2021.02.063. URL https://www.sciencedirect.com/science/article/pii/S0360319921005474.
25. Ahn B, Indlekofer T, Dawson JR and Worth NA. Heat release rate response of azimuthal thermoacoustic instabilities in a pressurized annular combustor with methane/hydrogen flames. *Combustion and Flame* 2022; 244: 112274. DOI:10.1016/j.combustflame.2022.112274. URL https://www.sciencedirect.com/science/article/pii/S0010218022002899.
26. Moon K, Choi Y and Kim KT. Experimental investigation of lean-premixed hydrogen combustion instabilities in a can-annular combustion system. *Combustion and Flame* 2022; 235: 111697. DOI:10.1016/j.combustflame.2021.111697.

URL https://www.sciencedirect.com/science/article/pii/S0010218021004405.

27. Abbot D, Giannotta A, Sun X, Gauthier P and Sethi V. Thermoacoustic Behaviour of a Hydrogen Micromix Aviation Gas Turbine Combustor Under Typical Flight Conditions 2021. American Society of Mechanical Engineers Digital Collection, p. 12. DOI:10.1115/GT2021-59844. URL https://asmedigitalcollection.asme.org/GT/proceedings-abstract/GT2021/84997/1120141.
28. Kang H and Kim KT. Combustion dynamics of multi-element lean-premixed hydrogen-air flame ensemble. *Combustion and Flame* 2021; 233: 111585. DOI: 10.1016/j.combustflame.2021.111585. URL https://www.sciencedirect.com/science/article/abs/pii/S001021802100328X. Publisher: Elsevier.
29. Lee T and Kim KT. High-frequency transverse combustion instabilities of lean-premixed multislit hydrogen-air flames. *Combustion and Flame* 2022; 238: 111899. DOI:10.1016/j.combustflame.2021.111899. URL https://linkinghub.elsevier.com/retrieve/pii/S0010218021006428.
30. Rajendram Soundararajan P, Durox D, Renaud A and Candel S. Impact of spray dynamics on combustion instabilities investigated by changing the atomizer recess in a swirl combustor. *Combustion and Flame* 2023; 252: 112757. DOI:10.1016/j.combustflame.2023.112757. URL https://www.sciencedirect.com/science/article/pii/S0010218023001414.
31. Palies P, Durox D, Schuller T and Candel S. Experimental Study on the Effect of Swirler Geometry and Swirl Number on Flame Describing Functions. *Combustion Science and Technology* 2011; 183(7): 704–717. DOI:10.1080/00102202.2010.538103. URL https://doi.org/10.1080/00102202.2010.538103. Publisher: Taylor & Francis _eprint: https://doi.org/10.1080/00102202.2010.538103.
32. Kim KT. Combustion instability feedback mechanisms in a lean-premixed swirl-stabilized combustor. *Combustion and Flame* 2016; 171: 137–151. DOI:10.1016/j.combustflame.2016.06.003. URL https://www.sciencedirect.com/science/article/pii/S0010218016301225.
33. Durox D, Moeck JP, Bourgouin JF et al. Flame dynamics of a variable swirl number system and instability control. *Combustion and Flame* 2013; 160(9): 1729–1742. DOI:10.1016/j.combustflame.2013.03.004. URL https://www.sciencedirect.com/science/article/pii/S0010218013000928.
34. Rajendram Soundararajan P, Durox D, Renaud A, Vignat G and Candel S. Swirler effects on combustion instabilities analyzed with measured FDFs, injector impedances and damping rates. *Combustion and Flame* 2022; 238: 111947. DOI:10.1016/j.combustflame.2021.111947. URL https://www.sciencedirect.com/science/article/pii/S0010218021006908.
35. Vaysse N, Durox D, Vicquelin R, Candel S and Renaud A. Stabilization and dynamics of pure hydrogen swirling flames using cross-flow injection 2023. Boston, USA: Paper No: GT2023-101977, p. 12.
36. Vaysse N, Durox D, Soundararajan PR, Vicquelin R, Candel S and Renaud A. Structure and light emission of swirling flames produced by pure hydrogen injection in cross-flow. In *Proceedings of the European Combustion Meeting* 2023. Rouen, France, p. 6.
37. Karyeyen S, Feser JS and Gupta AK. Hydrogen concentration effects on swirl-stabilized oxy-colorless distributed combustion. *Fuel* 2019; 253: 772–780. DOI:10.1016/j.fuel.2019.05.008. URL https://www.sciencedirect.com/science/article/pii/S0016236119307537.
38. Padley PJ. The origin of the blue continuum in the hydrogen flame. *Transactions of the Faraday Society* 1960; 56: 449. DOI: 10.1039/tf9605600449. URL http://xlink.rsc.org/?DOI=tf9605600449.
39. Fiala T and Sattelmayer T. Modeling of the continuous (blue) radiation in hydrogen flames. *International Journal of Hydrogen Energy* 2016; 41(2): 1293–1303. DOI:10.1016/j.ijhydene.2015.10.045. URL https://www.sciencedirect.com/science/article/pii/S036031991530505X.
40. Vignat G. *Injection and combustion dynamics in swirled spray flames and azimuthal coupling in annular combustors*. PhD Thesis, Université Paris-Saclay, 2021.